

High Accretion Rate during Class 0 Phase due to External Trigger

Kazutaka Motoyama[†] and Tatsuo Yoshida

Faculty of Science, Ibaraki University, Mito, Ibaraki 310-8521, Japan

27 August 2018

ABSTRACT

Recent observations indicate that some class 0 sources have orders of magnitude higher accretion rates than those of class I. We investigated the conditions for the high accretion rates of some class 0 sources by numerical calculations, modelling an external trigger. For no external trigger, we find that the maximum value of the accretion rate is determined by the ratio α of the gravitational energy to the thermal one within a flat inner region of the cloud core. The accretion rate reaches $\sim 10^{-4} M_{\odot} \text{yr}^{-1}$ if the cloud core has $\alpha \gtrsim 2$. For an external trigger we find that the maximum value of the accretion rate is proportional to the momentum given to the cloud core. The accretion rate reaches $\gtrsim 10^{-4} M_{\odot} \text{yr}^{-1}$ with a momentum of $\sim 0.1 M_{\odot} \text{km s}^{-1}$ when the initial central density of the cloud core is $\sim 10^{-18} \text{g cm}^{-3}$. A comparison between recent observational results for prestellar cores and our no triggered collapse model indicates that the flat inner regions of typical prestellar cores are not large enough to cause accretion rates of $\sim 10^{-4} M_{\odot} \text{yr}^{-1}$. Our results show that the triggered collapse of the cloud core is more preferable for the origin of the high accretion rates of class 0 sources than no triggered collapse.

Key words: hydrodynamics – circumstellar matter – stars: formation.

1 INTRODUCTION

Pre-main-sequence stars are classified according to their spectral features. Lada & Wilking (1984) and Lada (1987) proposed a classification for pre-main-sequence stars using the slope of their infrared Spectral Energy Distribution (SED). They insisted that this classification corresponds to an evolutional sequence. We state class I, II, and III in the order of evolution. In addition to these classifications, André, Ward-Thompson, & Barsony (1993) proposed a new category called class 0. The sub-mm ($\lambda > 350 \mu\text{m}$) luminosity of class 0 sources is 5×10^{-3} times higher than total luminosities, which indicates that class 0 sources are surrounded by significantly large amounts of circumstellar material. André & Montmerle (1994) insisted that class 0 sources are younger than those of class I.

The accretion rates of class 0 sources have been believed to be higher than those of class I by comparing the observations and theories. Bontemps et al. (1996) observed the CO outflow activities of YSOs nearby regions of star formation, and revealed that some class 0 sources have an order of magnitude larger momentum flux than those of class I. Most ejection models predict that the momentum flux of the outflow is proportional to the accretion rate (Pelletier

& Pudritz 1992; Wardle & Königl 1993; Shu et al. 1994). This means that these class 0 sources have higher accretion rates than those of class I. Moreover, Jayawardhana, Hartmann, & Calvet (2001) carried out radiative transfer calculations of infalling, dusty envelopes surrounding embedded protostars. They concluded that the prototype class 0 source VLA 1623 in the ρ Oph cloud must have an accretion rate $\gtrsim 10^{-4} M_{\odot} \text{yr}^{-1}$ by matching the far-infrared peak in the SED. This value is much higher than the typical accretion rates of $\sim 4 \times 10^{-6} M_{\odot} \text{yr}^{-1}$ of the class I sources in Taurus-Auriga, whose values were obtained by similar radiative transfer calculations (Kenyon, Calvet, & Hartmann 1993). Recently, Di Francesco et al. (2001) observed optically thick line $\text{H}_2\text{CO}(3_{12} - 2_{11})$ in the class 0 source NGC1333 IRAS 4A, and detected the inverse P-Cygni profile in the line. They derived a high infall velocity and a high accretion rate of $1.1 \times 10^{-4} M_{\odot} \text{yr}^{-1}$.

One possibility is that the high accretion rates of class 0 sources are related to the initial density profiles before gravitational collapses. If the starting point of star formation is a singular isothermal sphere (e.g. Shu, Adams, & Lizano 1987), the accretion rate is constant at $\sim c_s^3/G$ through the entire accretion phase, where c_s and G denote the sound speed and the gravitational constant, respectively. The time variation of the accretion rate can be caused by an initial density profile different from that of a

[†] E-mail: motoyama@golf.sci.ibaraki.ac.jp

singular isothermal sphere (Foster & Chevalier 1993; Henriksen, André & Bontemps 1997 hereafter HAB; Whitworth & Ward-Thompson 2001). HAB reproduced high accretion rates of class 0 sources by assuming that a prestellar core has a flat inner region surrounded by a power-law envelope. In their model, the accretion rate is high in the earlier accretion phase, and declines later. Their model is consistent with the picture that the accretion rates of class 0 sources are higher than those of class I.

In this paper we investigate quantitatively the conditions for the high accretion rates of class 0 sources based on hydrodynamic calculations. When we take into account the pressure effect, even though the analytic HAB's model neglects it, we must assume that the flat inner regions is more massive in order to cause high accretion rates. Recent observations reveal both the masses and sizes of the flat inner regions of prestellar cores (Ward-Thompson, Motte, and André 1999). Assuming a gas temperature of 10 K, the flat inner regions of typical prestellar cores have thermal energies that are comparable to the gravitational ones. It seems that such cores do not cause high accretion rates.

We have investigated collapses with and without an external trigger. If star formation is triggered by an interstellar shock wave, a high accretion rate is expected due to compression by the shock wave. The cloud cores interact with the shock wave under various circumstances. For instance, triggered star formation by a distant supernova is suggested in the Upper Sco association (Walter et al. 1994; Preibisch & Zinnecker 1999) and the ρ Oph cloud (Vrba 1977; Loren & Wootten 1986; de Geus 1992; Preibisch & Zinnecker 1999). The star formation in NGC 2265 IRS in the Cone Nebula seems to be triggered by stellar wind from a B2 star (Thompson et al. 1998). The triggered formation scenario is also proposed for the origin of the solar system based on studies of meteorites (Cameron & Truran 1977). The presence of short-lived isotopes in meteorites, which should be provided by stellar ejecta from a supernova, or an asymptotic giant branch star, leads to this scenario.

Many numerical simulations have been carried out to investigate the triggered collapse scenario (Boss 1995; Foster & Boss 1996; Vanhala & Cameron 1998). Hennebelle et al. (2002) investigated the evolutions of a Bonnor-Ebert sphere which is subjected to an increase in the external pressure. They demonstrated that the features of the density and velocity field of prestellar cores and protostars are well reproduced, and that the accretion rate is high in the earlier accretion phase. In this paper, we examine the possibility that an external trigger causes a high accretion rate of $\sim 10^{-4} M_{\odot} \text{yr}^{-1}$. We investigate the conditions for the high accretion rates of class 0 sources, pursuing numerical calculations of the collapse of the cloud core triggered impulsively by an external shock wave.

In Section 2, we describe our models and numerical method. In Section 3, we present the numerical results. In Section 4, we summarize the main results and discuss them.

2 MODELS AND NUMERICAL METHOD

2.1 Basic equations and models

The fluid equations in spherical coordinates are

$$\frac{d\rho}{dt} + 4\pi\rho^2 \frac{\partial}{\partial m}(r^2 v) = 0, \quad (1)$$

$$\frac{dv}{dt} = -4\pi r^2 \frac{\partial P}{\partial m} - \frac{Gm(r)}{r^2}, \quad (2)$$

where ρ is the density, v the radial velocity, P the pressure, and m the mass within radius r ,

$$m(r) = \int_0^r 4\pi r'^2 \rho(r') dr'. \quad (3)$$

Although the density of the cloud core increases drastically in the process of star formation, radiative cooling is effective except for the high-density region in the centre (Larson 1969). We assume that the medium is an isothermal gas,

$$P = c_s^2 \rho. \quad (4)$$

The gas temperature T is set at 10 K ($c_s = 215 \text{ m s}^{-1}$), which is the typical temperature for globules and cloud cores (e.g. Clemens, Yun, and Heyer 1991) in our calculations. The mean molecular weight and the ratio of the specific heats are set at 2.5 (assuming cosmic abundance) and 7/5, respectively.

We adopt a Plummer-like density profile as an initial condition (Whitworth & Ward-Thompson 2001). Recent high angular resolution observations of the precollapse cloud support this Plummer-like density profile. Ward-Thompson et al. (1994) demonstrated that prestellar cores have flat inner regions surrounded by power-law envelopes based on the observation of starless NH₃ cores. We assume the following initial density profile:

$$\rho_0(r) = \rho_{flat} \left[\frac{R_{flat}}{(R_{flat}^2 + r^2)^{\frac{1}{2}}} \right]^{\eta}. \quad (5)$$

At a radius smaller than R_{flat} , the density is nearly constant, ρ_{flat} . At a radius larger than R_{flat} , the density is proportional to $r^{-\eta}$. We fix the parameter $\eta = 2$ in our models presented in section 3.

2.2 Numerical methods

We solved numerically equations (1)-(4) using a finite difference scheme. These equations were integrated by Godunov's method. This Lagrangian hydrodynamical code has a second order accuracy in both space and time. We set the inner ($r = 0$) boundary conditions such that P and ρ have a zero gradient, and $v = 0$, and the outer boundary conditions that P , ρ , and v have a zero gradient. We used the non-uniform grids, $\Delta m_{i+1} = (1 + \epsilon) \Delta m_i$, where Δm_i is the mass inside the i th grid from the centre. The value of ϵ was set at 3×10^{-3} in order to obtain a high resolution at the centre. We used 6000 grids in our calculations. For the cloud core itself of the mass $3 M_{\odot}$, 2737 grids were allocated. Outside of the cloud core, the density is equal to that of core edge, and the gravitational force was excluded from our calculation.

We used the sink-cell method adopted by Boss & Black (1982) to calculate the later accretion phase. In many numerical simulations which treated the collapse of the isothermal sphere, the density and the infall velocity of the central region increase drastically during a runaway collapse phase. It is difficult to continue calculations to a later stage, because the time step that satisfies the CFL condition is too small.

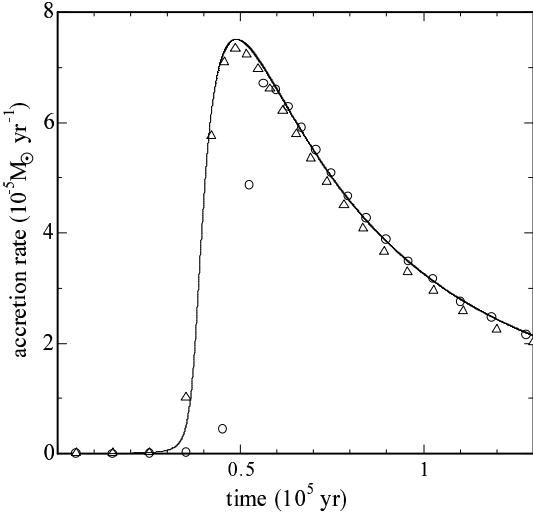


Figure 1. Accretion rate as a function of time. The solid line denotes the analytic solution given by Whitworth & Ward-Thompson (2001). The circles and the triangles denote the case of $T = 10$ K and $T = 0.5$ K, respectively.

When the central density reaches a reference density value, ρ_{sink} , cells within radius r_{sink} are treated as sink-cells: the accreted gas into sink-cells is treated as point like mass at the centre. Since the infall velocity near the sink-cell exceeds the sound velocity, the effect of the sink-cell does not travel to the outer gas.

As a test for the numerical code, we compared our result with the analytic solution of Whitworth & Ward-Thompson (2001). We evaluated the accretion rate at the radius $r_{acc} = 300$ AU. Fig. 1 shows comparison between the analytic solution and our results. Each parameter was set as follows: $\rho_{flat} = 3.0 \times 10^{-18}$ g cm $^{-3}$, $R_{flat} = 5350$ AU, and $\eta = 4$. The gas temperatures are set at 10 K and 0.5 K. The result in the case of $T = 0.5$ K agrees well with the analytic solution. On the other hand, in the case of $T = 10$ K, the maximum value of accretion rate is less than that of the analytic solution because of a pressure effect.

3 RESULTS

We studied two different models in order to seek for the conditions for a high accretion rate of $\sim 10^{-4} M_{\odot} \text{yr}^{-1}$. In Section 3.1 and Section 3.2, we consider the collapse of cloud core without and with an external trigger, respectively. We call the former the no triggered collapse model, and the latter triggered collapse model in this paper.

3.1 No triggered collapse model

Here, we present the numerical results of the no triggered collapse model. We summarize the model parameters and the maximum value of accretion rate in Table 1. Fig. 2 and Fig. 3 show the evolutions of the density and the velocity profiles in model A1. Here, we use the time $\tau = t / t_{ff}$, which is normalized by the initial free fall time, $t_{ff} = \left(\frac{3\pi}{32G\rho_{flat}} \right)^{1/2}$, at the centre. In the runaway collapse phase

Table 1. Model parameters and the maximum value of accretion rate \dot{M}_{max} for the no triggered collapse model.

| model | ρ_{flat} (g cm $^{-3}$) | R_{flat} (AU) | M_{flat} (M_{\odot}) | α | \dot{M}_{max} ($M_{\odot} \text{yr}^{-1}$) |
|-------|----------------------------------|--------------------|-------------------------------|----------|---------------------------------------------------|
| A1 | 1.0×10^{-18} | 3400 | 0.18 | 0.42 | 4.27×10^{-5} |
| A2 | 1.0×10^{-16} | 710 | 0.18 | 1.8 | 1.82×10^{-4} |
| B1 | 1.0×10^{-18} | 4300 | 0.36 | 0.67 | 5.45×10^{-5} |
| B2 | 1.0×10^{-16} | 930 | 0.36 | 3.1 | 3.88×10^{-4} |
| C | 2.0×10^{-18} | 4200 | 0.67 | 1.3 | 9.77×10^{-5} |
| D1 | 1.0×10^{-18} | 8000 | 2.3 | 2.3 | 1.59×10^{-4} |
| D2 | 1.0×10^{-16} | 1720 | 2.3 | 11 | 1.56×10^{-3} |

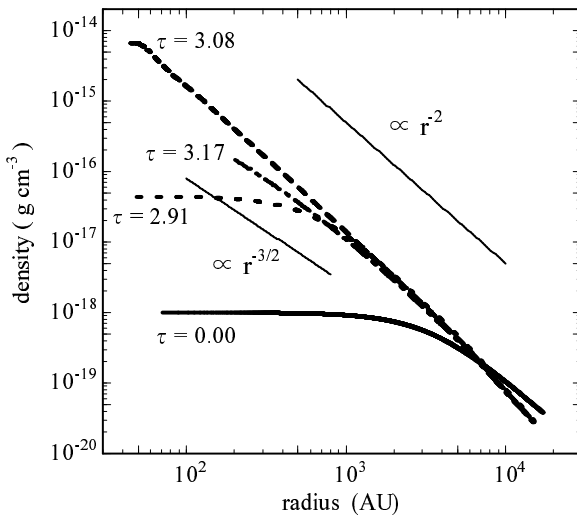


Figure 2. Evolution of the density profile in model A1. The number attached to each line denotes the time normalized by the initial free fall time at the centre.

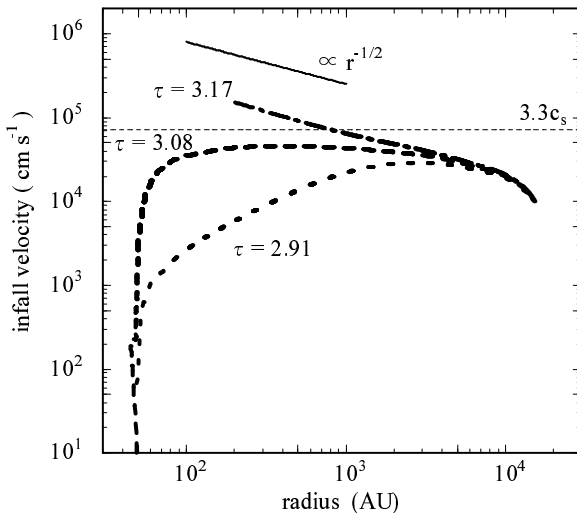


Figure 3. Evolution of the velocity profile in model A1. The number attached to each line is the same as in Fig. 2.

$(\tau < 3.09)$, the flat inner region shrinks and its density increases as the collapse proceeds. The density is proportional to r^{-2} in the outer envelope. The infall velocity is nearly uniform at $\sim 3.3 c_s$ in the outer region. After core formation ($\tau > 3.09$), the density and the infall velocity are proportional to $r^{-3/2}$ and $r^{-1/2}$ in the central region, respectively.

Fig. 4 shows the accretion rates of each model as a function of the envelope mass, which is used as an evolutionary indicator. The envelope mass denotes the mass that remains outside of radius r_{acc} . In all models, the accretion rates increase rapidly during the earlier collapse phases. After the accretion rate reaches the maximum value, \dot{M}_{max} , it gradually declines. The maximum value of accretion rate increases as the ratio α of the gravitational energy to the thermal one within the inner flat region is large. Fig. 4 indicates that the value of α is larger than 2 in order to cause an accretion rate of $\sim 10^{-4} M_\odot \text{yr}^{-1}$. We compared our results with the accretion rates of the pressure-free models. For models with $\alpha \gtrsim 2$, the maximum values of the accretion rates can be fitted well with pressure-free solutions.

We can estimate the accretion rate for a larger α , neglecting pressure effect. The inner flat region with mass M_{flat} collapses within

$$\Delta t = \overline{t_{ff}}(R_{flat}) - t_{ff} = \left(1 - \frac{\sqrt{3(4-\pi)}}{2}\right) \overline{t_{ff}}(R_{flat}), \quad (6)$$

where $\overline{t_{ff}}(R_{flat})$ represents the free fall time of the mean density, $\overline{\rho}(R_{flat}) = [4\pi\rho_{flat}R_{flat}^3(1-\frac{\pi}{4})]/(\frac{4}{3}\pi R_{flat}^3)$, within the radius R_{flat} . The accretion rate is given by

$$\dot{M} \sim \frac{M_{flat}}{\Delta t} \quad (7)$$

$$= \frac{2}{\pi \left(1 - \frac{\sqrt{3(4-\pi)}}{2}\right)} \left(\frac{2GM_{flat}^3}{R_{flat}^3}\right)^{1/2}. \quad (8)$$

If we consider the inner flat region as approximately an uniform sphere, the ratio α is estimated to be

$$\begin{aligned} \alpha &\sim 2GM_{flat}/(5c_s^2 R_{flat}) \\ &\sim 0.42 \left(\frac{M_{flat}}{0.18 M_\odot}\right) \left(\frac{R_{flat}}{3400 \text{AU}}\right)^{-1} \left(\frac{T}{10 \text{K}}\right)^{-1}. \end{aligned} \quad (9)$$

Substituting this relation into equation (8) gives

$$\dot{M} \sim 4.24 \times 10^{-5} \alpha^{3/2} \left(\frac{T}{10 \text{K}}\right)^{3/2} M_\odot \text{yr}^{-1}. \quad (10)$$

This estimation neglecting pressure effect is appropriate for the cases with $\alpha \gtrsim 2$. Then, the accretion rates are essentially determined by R_{flat} and M_{flat} , although equation (10) seems to depend on T . A similar estimation is also found in Ogino, Tomisaka, & Nakamura (1999).

3.2 Triggered collapse model

Here, we present numerical results of the triggered collapse model. We give some grids outside of the cloud core the velocity to a centre, v_{ini} . The total amount of mass in these grids is M_{ini} . A similar method is used in Boss (1995). We summarize the model parameters, the arrival times at the centre of shock waves t_s , and the maximum values of the

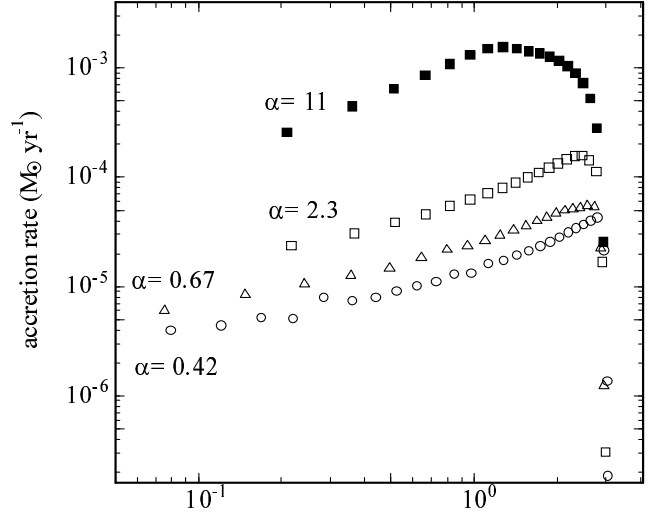


Figure 4. Accretion rate as a function of the envelope mass. The open circles, open triangles, open squares, and filled squares denote model A1, B1, D1, and D2, respectively. The number attached to each plot denotes the ratio α of the gravitational energy to the thermal one within the inner flat region.

Table 2. Model parameters, the arrival times at the centre of shock waves t_s , and the maximum values of the accretion rate for triggered collapse models. The value of the initial free fall time at the centre t_{ff} is $6.65 \times 10^4 \text{yr}$ in the case of $\rho_{flat} = 1.0 \times 10^{-18} \text{g cm}^{-3}$.

| model | v_{ini} (km s^{-1}) | M_{ini} ($10^{-2} \times M_\odot$) | t_s ($\times t_{ff}$) | \dot{M}_{max} ($M_\odot \text{yr}^{-1}$) |
|-------|-------------------------------------|-------------------------------------------|------------------------------|-------------------------------------------------|
| D3 | 3 | 0.9 | 3.16 | 6.73×10^{-5} |
| E5 | 5 | 1.8 | 2.93 | 1.09×10^{-4} |
| E10 | 10 | 1.8 | 2.61 | 1.10×10^{-4} |
| E15 | 15 | 1.8 | 2.35 | 1.23×10^{-4} |
| E20 | 20 | 1.8 | 2.15 | 1.34×10^{-4} |
| F5 | 5 | 3.6 | 2.63 | 1.11×10^{-4} |
| F10 | 10 | 3.6 | 2.16 | 1.40×10^{-4} |
| F15 | 15 | 3.6 | 1.84 | 1.99×10^{-4} |
| F20 | 20 | 3.6 | 1.60 | 2.65×10^{-4} |
| G10 | 10 | 4.5 | 1.99 | 1.63×10^{-4} |
| G15 | 15 | 4.5 | 1.68 | 2.47×10^{-4} |

accretion rates in Table 2. We adopt the density distribution of model A1 as an initial condition, of which α is the smallest in no triggered collapse models.

Fig. 5 and Fig. 6 show the evolutions of the density and the velocity profiles in model E20, respectively. While the shock front propagates to the centre ($\tau < 2.14$), the shock wave compresses the envelope gas. As a result, the cloud core has a centrally concentrated configuration relative to the initial state. The density of this region is approximately uniform and one order higher than the density of the preshock region, where the shock wave has not yet arrived, and the density profile of the outer region is steeper than $\propto r^{-2}$. The propagating speed of the shock front is nearly constant during compression. The velocity of the preshock region is nearly at rest, and the velocity of the postshock region is uniform. Compared with no triggered model, the envelopes

are denser and have steeper outer-regions during the earlier collapse phases, which correspond to the class 0 phases.

Fig. 7 represents the accretion rate in model E20 compared with model A1. In model E20, the accretion rate takes the maximum value ($\tau = 2.24$) just after the collapse of the flat inner region. After that, the accretion rate declines rapidly. In the later phase there is no large difference between the accretion rates of model A1 and model E20. Other models have the same time evolution as model E20.

Our results suggest that the maximum values of the accretion rates are proportional to momenta given to the cloud cores. Fig. 8 plots the maximum values of the accretion rates versus the momenta given to the cloud cores, $M_{ini}v_{ini}$. The models with the same momenta show similar values of \dot{M}_{max} and t_s : i.e., E10 and F5, E20 and F10. The maximum value of accretion rate is determined by the momentum given to the cloud core. A momentum $\gtrsim 0.1M_{\odot}\text{km s}^{-1}$ causes an accretion rate of $\gtrsim 10^{-4}M_{\odot}\text{yr}^{-1}$.

The maximum value of the accretion rate can be estimated as follows. From equation (9), α of the centrally concentrated flat region compressed by external shock wave is

$$\alpha \sim \frac{2G}{5c_s^2} \frac{M_{com}}{R_{com}}. \quad (11)$$

Here, M_{com} and R_{com} denote the mass and the radius of this compressed region, respectively. If the arrival time at the centre of the shock wave t_s is shorter than the time t_{nt} , when the central density reaches ρ_{sink} , for the no triggered case (i.e. model A1), we can assume that the density and the velocity of the preshock region remain unchanged from the initial state. Using the relation of the compression ratio for isothermal shock, we obtain $\rho_{com}/\rho_{flat} \sim (v_{com}/c_s)^2$, where ρ_{com} and v_{com} denote the density and the velocity of the compressed region, respectively. Thus, equation (11) is rewritten as

$$\alpha \sim \frac{2G}{5c_s^2} \left(\frac{4\pi\rho_{flat}}{3c_s^2} \right)^{1/3} (M_{com}v_{com})^{2/3}. \quad (12)$$

The momentum within the compressed flat region is conserved if the impulse I_{pre} given from the preshock region is negligible. This impulse

$$I_{pre} = \int_0^{t_s} 4\pi r_s^2 c_s^2 \rho_0(r_s) dt \quad (13)$$

is negligible compared with $M_{ini}v_{ini}$, assuming a constant velocity of the shock front (i.e. $r_s = R_c(1 - t/t_s)$), where r_s and $R_c = 1.7 \times 10^4$ AU denotes the distance from the centre to the shock front and the radius of the cloud core, respectively. We can replace $M_{com}v_{com}$ with $M_{ini}v_{ini}$ in equation (12). Substituting this relation into equation (10) gives

$$\dot{M} \sim 3.52 \times 10^{-4} \left(\frac{M_{ini}v_{ini}}{1 M_{\odot}\text{km s}^{-1}} \right) \left(\frac{\rho_{flat}}{10^{-18} \text{g cm}^{-3}} \right)^{1/2} \times \left(\frac{T}{10 \text{K}} \right)^{-1/2} M_{\odot}\text{yr}^{-1}. \quad (14)$$

As shown Fig. 8, our results are classified into three categories according to the comparison between the arrival time at the centre of the shock wave t_s and the required time for the central density to reach ρ_{sink} , $t_{nt} = 3.11 t_{ff}$. In the case of $t_s \ll t_{nt}$ ($M_{ini}v_{ini} \gtrsim 0.3M_{\odot}\text{km s}^{-1}$), our numerical results agrees well with the relation of equation

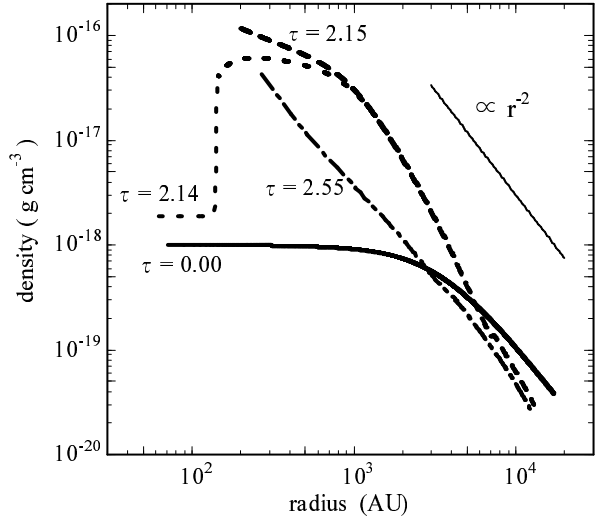


Figure 5. Evolution of the density profile in model E20. The number attached to each line is the same as in Fig. 2.

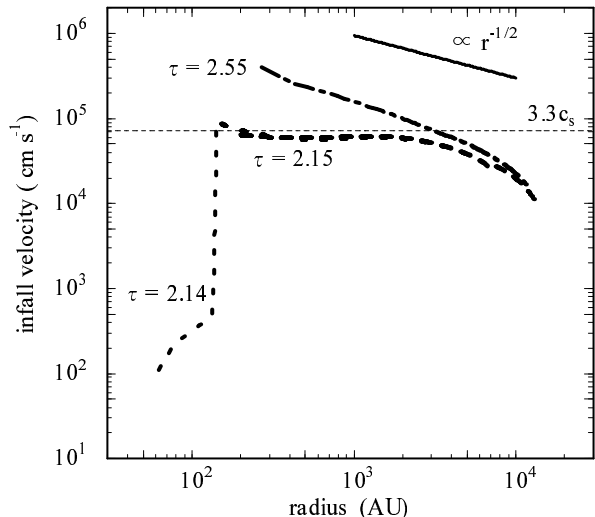


Figure 6. Evolution of the velocity profile in model E20. The number attached to each line is the same as in Fig. 2.

(14). In the case of $t_s \sim t_{nt}$ ($0.05M_{\odot}\text{km s}^{-1} \lesssim M_{ini}v_{ini} \lesssim 0.3M_{\odot}\text{km s}^{-1}$), the maximum values of the accretion rates are higher than the relation of equation (14), because there are effects of both compression by the shock wave and contraction by self-gravity. In the case of $t_s > t_{nt}$ ($M_{ini}v_{ini} \lesssim 0.05M_{\odot}\text{km s}^{-1}$), the effect of the compression by the shock wave is small.

4 SUMMARY AND DISCUSSION

We summarize our main results as follows:

- (i) The collapse of cloud core with $\alpha \gtrsim 2$ can be treated as pressure-free, and the maximum value of the accretion rate is proportional to $\alpha^{3/2}$ in the no triggered collapse, where α is the ratio of the gravitational energy to the thermal one

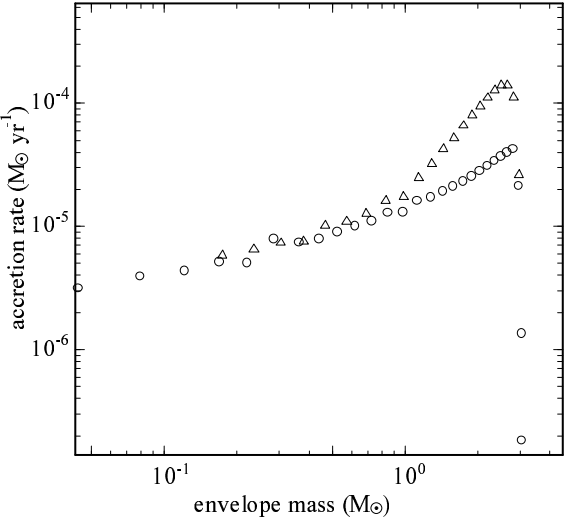


Figure 7. Accretion rates as a function of the envelope mass. The open circles and the open triangles denote models A1 and E20, respectively.

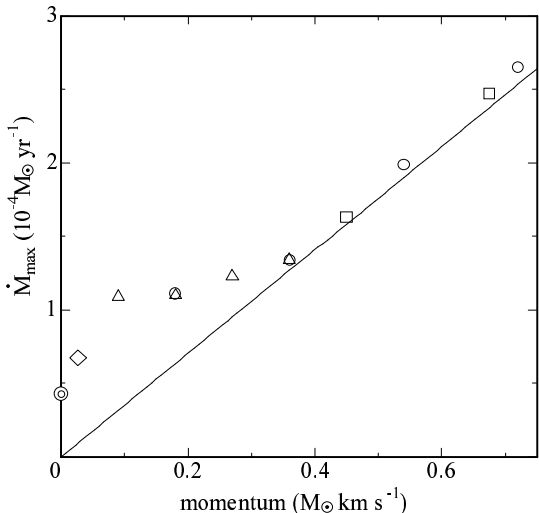


Figure 8. Maximum values of the accretion rates \dot{M}_{max} versus the momenta given to cloud cores, $M_{ini}v_{ini}$. The double open circle denotes model A1. The open diamond denotes model D3. The open triangles denote models E5, E10, E15, and E20. The open circles denote models F5, F10, F15, and F20. The open squares denote models G10 and G15. The solid line denotes the relation of equation (14).

within the flat inner region of the cloud core. A flat inner region with $\alpha \gtrsim 2$ causes an accretion rate of $\gtrsim 10^{-4} M_{\odot} \text{yr}^{-1}$.

(ii) For triggered collapse, the cloud core has a centrally concentrated configuration relative to the initial state as the result of compression by the shock wave. Just after the shock front reaches the centre, when the cloud core has compressed the flat inner region and outer steep envelope, the accretion rate attains the maximum value.

(iii) The maximum value of the accretion rate is proportional to the momentum given to the cloud core in the triggered collapse. The momentum $\gtrsim 0.1 M_{\odot} \text{km s}^{-1}$ causes an

accretion rate of $\gtrsim 10^{-4} M_{\odot} \text{yr}^{-1}$ when the initial central density of the cloud core, ρ_{flat} , is $\sim 10^{-18} \text{g cm}^{-3}$.

Hennebelle et al. (2003) investigated the evolutions of a Bonnor-Ebert sphere which is subjected to an increase in the external pressure with Smoothed Particle Hydrodynamics simulations. Their simulations indicate that the prestellar core has a flat inner region and a steep outer envelope, and approximately a uniform infall velocity profile. Their results for the fast compression cases, $\phi < 1$, are similar to ours concerning the density and the velocity profiles, where their parameter ϕ is defined as the ratio of the time scale on which the external pressure doubles to the initial sound crossing time. These features are consistent with observations of prestellar cores. However, in their calculations the maximum value of the accretion rate reaches only $\sim 3 \times 10^{-5} M_{\odot} \text{yr}^{-1}$. This low accretion rate is due to their low initial central density, $\rho_{flat} \sim 6 \times 10^{-20} \text{g cm}^{-3}$, which is two orders lower than that of our model, $\rho_{flat} = 10^{-18} \text{g cm}^{-3}$.

We discuss the masses and the sizes of the flat inner regions of prestellar cores. Although in the ρ Oph cloud there is a high-accretion class 0 source, i.e. VLA 1623, a comparison between the observational results and our no triggered collapse model indicates that the flat inner regions of prestellar cores are not large enough to cause accretion rates of $\gtrsim 10^{-4} M_{\odot} \text{yr}^{-1}$. The mass and the radius of the flat inner region of the prestellar core L1689B in the ρ Oph complex are estimated to be $\sim 0.33 M_{\odot}$ and $\sim 4000 \text{AU}$ (André, Ward-Thompson, & Motte 1996). The parameters of this prestellar core nearly coincide with those of model B1, in which the accretion rate and α are $5.45 \times 10^{-5} M_{\odot} \text{yr}^{-1}$ and 0.67, respectively. Moreover, Ward-Thompson et al. (1999) recently observed eight isolated prestellar cores. They estimated the typical mass and the radius of the flat inner regions to be $\sim 0.7 M_{\odot}$ and $\sim 4000 \text{AU}$. The parameters of this prestellar core nearly coincide with those of model C, in which the accretion rate and α are $9.77 \times 10^{-5} M_{\odot} \text{yr}^{-1}$ and 1.3, respectively. These results indicate the difficulty of evolution from the typical prestellar core into the observed high-accretion class 0 source without an external trigger.

In regions where stars form in cluster, some observational results indicate the triggered collapse scenario. Tachihara et al. (2002) found that clouds with cluster formation have head-tail structures, studying statistically 179 cloud cores in nearby star-forming regions. Such structures indicate interactions with the external shock wave. Moreover, the class 0 envelopes in Perseus are 3 to 12 times denser than singular isothermal sphere at $T = 10 \text{ K}$ (Motte and André 2001). The high density of class 0 sources can be interpreted as being the results of compression by an external shock wave. These facts suggest that star formations are caused by external triggers in these regions.

Momentum plays an important role in triggered star formation. Foster & Boss (1996) investigated the interaction of a plane wave and the cloud core by two-dimensional calculations. They showed that a fast adiabatic shock wave is liable to disrupt the cloud core, and that a slow isothermal shock wave causes a collapse of the cloud core. They also showed that the momentum given to the cloud core is more essential than the kinetic energy in predicting whether induced collapse occurs or not.

Next, we discuss the magnitude of the momentum in triggered collapse. Foster & Boss (1996) estimated the momentum given to the cloud core by an explosion with an initial kinetic energy of $E = 2 \times 10^{50}$ erg. They assumed that the evolution of a remnant switches from the Sedov-Taylor expansion phase to an isothermal expansion phase at a shell temperature of 10^6 K. They adopted a mean molecular weight of $\mu = 0.61$. This switch occurs at a radius of $\sim 14 \text{ pc} (E/2 \times 10^{50} \text{ erg})^{1/3} (n/1 \text{ cm}^{-3})^{-1/3}$. The momentum impacting on the cloud core at a distance $R = 29$ pc from a supernova is estimated to be $\sim 0.1 M_{\odot} \text{ km s}^{-1} (E/2 \times 10^{50} \text{ erg}) (R_c/1.7 \times 10^4 \text{ AU})^2 (R/29 \text{ pc})^{-2}$, where R_c is the radius of the cloud core in our triggered collapse model. Therefore, a supernova located up to 29 pc away from cloud cores would cause a high accretion rate of $\gtrsim 10^{-4} M_{\odot} \text{ yr}^{-1}$. Although the cloud core is impacted by a planar shock in this situation, our calculation is spherically symmetric. If the pressure of the post-shock region is sufficiently comparable to that of the cloud core, and the shock wave does not significantly compress before the shock front passes the core (i.e. $t_s > 2R_c/v_{ini}$), the cloud core would be spherically compressed. Otherwise, the cloud core would be compressed from one side (Lim, Hartquist, & Williams 2001). The accretion rate would have a somewhat lower value than in the case of spherically symmetry. In the ρ Oph cloud scenarios of shock triggered star formation suggested by many authors (Vrba 1977; Loren & Wootten 1986; de Geus 1992; Preibisch & Zinnecker 1999), an expanding shell of H I gas created by a supernova in the Sco OB2 association induces star formation in the ρ Oph cloud at a distance of about 20 pc from the Upper-Scorpius subgroup of the Sco OB2.

We have investigated the conditions for the high accretion rates of class 0 sources. Our results indicate that it is difficult to cause a high accretion rate of $\gtrsim 10^{-4} M_{\odot} \text{ yr}^{-1}$ with no triggered collapses of typical prestellar cores. For no triggered collapse, the flat inner region of prestellar core must be $\alpha \gtrsim 2$ in order to cause this high accretion rate. Otherwise, an external trigger is necessary for a high accretion rate. Future high-resolution observations (e.g. ALMA) will reveal the detailed density and velocity structures of prestellar and protostellar cores. Observations with high velocity resolution give accurate accretion rates of protostars from their line profiles. If we know the detailed structures of the envelopes and accretion rates of class 0 sources simultaneously, it would reveal whether an external trigger affect the accretion rate.

ACKNOWLEDGEMENTS

We thank an anonymous referee for many helpful comments concerning our manuscript.

REFERENCES

André P., Montmerle T., 1994, ApJ, 420, 837
 André P., Ward-Thompson D., Barsony M., 1993, ApJ, 406, 122
 André P., Ward-Thompson D., Motte F., 1996, A&A, 314, 625
 Bontemps S., André P., Terebey S., Cabrit S., 1996, A&A, 311, 858
 Boss A. P., 1995, ApJ, 439, 224
 Boss A. P., Black D. C., 1982, ApJ, 258, 270

Cameron A. G. W., Truran J. W., 1977, Icarus, 30, 447
 Clemens D. P., Yun M. L., Heyer M. H., 1991, ApJS, 75, 877
 de Geus E. J., 1992, A&A, 262, 258
 Di Francesco J., Myers P. C., Wilner D. J., Ohashi N., Mardones D., 2001, ApJ, 562, 770
 Foster P. N., Boss A. P., 1996, ApJ, 468, 784
 Foster P. N., Chevalier R. A., 1993, ApJ, 416, 303
 Hennebelle P., Whitworth A. P., Gladwin P. P., André P., 2003, MNRAS, 340, 870
 Henriksen R., André P., Bontemps S., 1997, A&A, 323, 549 - HAB
 Jayawardhana R., Hartmann L., Calvet N., ApJ, 2001, 548, 310
 Kenyon S. J., Calvet N., Hartmann L., 1993, ApJ, 414, 676
 Lada C. J., 1987, in Peimbert M., Jugaku J. eds, Proc. IAU Symp. 115, Star Forming Regions, Reidel, Dordrecht, p.1
 Lada C. J., Wilking B. A., 1984, ApJ, 287, 610
 Larson R. B., 1969, MNRAS, 145, 271
 Lim A. J., Hartquist T. W., Williams D. A., 2001, MNRAS, 326, 1110
 Loren R. B., Wootten A., 1986, ApJ, 306, 142
 Motte F., André P., 2001, A&A, 396, 440
 Ogino S., Tomisaka K., Nakamura F., 1999, PASJ, 51, 637
 Pelletier G., Pudritz R. E., 1992, ApJ, 394, 117
 Preibisch T., Zinnecker H., 1999, AJ, 117, 2381
 Shu F., Adams F.C., Lizano S., 1987, ARA&A 25, 23
 Shu F., Najita J., Ostriker E., Wilkin F., Ruden S., Lizano S., 1994, ApJ, 429, 781
 Tachihara K., Onishi T., Mizuno A., Fukui Y., 2002, A&A, 385, 909
 Thompson R. I., Corbin M. R., Young E., Schneider G., 1998, ApJ, 492, L177
 Vanhala H. A. T., Cameron A. G. W., 1998, ApJ, 508, 291
 Vrba F. J., 1977, AJ, 82, 198
 Walter F. M., Vrba F. J., Mathieu R. D., Brown A., Myers P.C., 1994, AJ, 107, 692
 Ward-Thompson D., Scott P. F., Hills R. E., André P., 1994, MNRAS, 268, 276
 Ward-Thompson D., Motte F., André P., 1999, MNRAS, 305, 143
 Wardle M., Königl A., 1993, ApJ, 410, 218
 Whitworth A. P., Ward-Thompson D., 2001, ApJ, 547, 317